Applied Catalysis A: General 359 (2009) 165–179

Contents lists available at ScienceDirect

Applied Catalysis A: General

journal homepage: www.elsevier.com/locate/apcata

Studies of catalytic activity and coke deactivation of spinel oxides during ethylbenzene dehydrogenation

Rafael M. Freire [a,1], Francisco F. de Sousa [b,2], Anderson L. Pinheiro [a,1], Elisane Longhinotti [a,1], J. Mendes Filho [b,2], Alcemira C. Oliveira [c,3], Paulo de Tarso C. Freire [b,2], Alejandro P. Ayala [b,2], Alcineia C. Oliveira [a,*]

[a] Universidade Federal do Ceará, Campus do Pici-Bloco 940, Langmur Lab. de Adsorção e Catálise, 60.000.000, Fortaleza, Ceará, Brazil
[b] Universidade Federal do Ceará, Campus do Pici-Bloco 922, Departamento de Física, Fortaleza, Ceará, Brazil
[c] Universidade Federal da Bahia, Instituto de Física Campus Universitário da Federação, 40210-340 579 Salvador, Bahia, Brazil

ARTICLE INFO

Article history:
Received 13 January 2009
Received in revised form 18 February 2009
Accepted 20 February 2009
Available online 3 March 2009

Keywords:
Spinel oxides
Ethylbenzene
Dehydrogenation
CO_2
Coking

ABSTRACT

Catalytic dehydrogenation of ethylbenzene with CO_2 to produce styrene was carried out on MAl_2O_4 (where M = Cu^{2+}, Ni^{2+}, or both), and also with pure NiO and CuO catalysts. The synthesized materials were characterized by various physico-chemical techniques and catalytic activity, coke deactivation, and recycling of spent catalysts were studied. The $NiAl_2O_4$ phase showed the highest activity under moderate conditions (activity = 160×10^{-3} mol g^{-1} h^{-1}; selectivity to styrene = 90.7%). Pure NiO and CuO were virtually inactive in the reaction due to the easy reduction of the phases in these oxides. $NiAl_2O_4$, an active phase for the reaction, was cooperatively associated with Cu in a highly stable ternary system (Cu-Ni-Al). However, this association did not result in high conversion or selectivity. Analyses of the coked catalysts revealed the presence of carbon on the solid surface that was in the form of graphite and polyaromatics. Deactivation studies on $NiAl_2O_4$ proved that Ni^{2+} sites were covered with a moderate amount of crystalline graphite that grew progressively and was subsequently eliminated by using higher CO_2/EB ratios. These results suggest that a reverse water shift reaction may be occurring when this solid is used. On the other hand, polyaromatic carbons were not eliminated and were the leading cause of the catalyst deactivation, rather than the physical degradation (reduction) of the solid. Recycling studies have demonstrated the high tendency of $NiAl_2O_4$ to regain the oxidation state of nickel, and thus, the styrene selectivity was maintained for over 40 h. The conditions leading to the highest conversion were a CO_2/EB ratio of 30 and a T = 550 °C at ambient pressure. Under these conditions, activities were comparable to those of Fe-K commercial catalysts for dehydrogenation, leading over the steam.

1. Introduction

Since the mid-1930s, the subject of catalysts for styrene production has received increasing interest [1–7]. The advances in this area have been driven by the need for producing valuable commodities from styrene, such as thermoplastics, fibers, polymers, and resins. The most important commercial route for styrene production is the catalytic dehydrogenation of ethylbenzene at high temperatures (600–700 °C) in the presence of promoting iron oxide catalysts and a large quantity of steam [1,8].

However, it is well known that the commercial process wastes large quantities of latent heat of steam condensation, and the conversions obtained are low due to the thermodynamic equilibrium limitation [2–8]. In addition to this, the typical Fe-K oxide-based catalyst used for the commercial dehydrogenation process does not work efficiently, although it has been successfully improved by either physical mixing or chemical incorporation of various promoters.

Recently, much attention has been devoted to developing a new catalysis process to make styrene production more economical and environmentally friendly. Thus, the utilization of CO_2, which is a mild oxidant and greenhouse gas, has aroused increasing interest. For that reason, several investigations have been carried out on the dehydrogenation of ethylbenzene in the presence of CO_2 [7,9–12].

No commercial technology for CO_2 dehydrogenation of ethylbenzene has been developed so far because no catalysts have been found to be effective, stable, and resistant to coke formation. A variety of catalysts, such as metal and/or alkali-promoters on pillared clays, hydrotalcites, zeolites, and oxides, have been investigated. Indeed, Fe, V, Zr, Ti, Cr, Ce, Al, Mn, Mg, Mo,

* Corresponding author. Tel.: +55 85 33 66 90 51; fax: +55 85 33 66 90 82.
E-mail address: alcineia@ufc.br (A.C. Oliveira).
[1] Tel.: +55 85 33 66 90 41; fax: +55 85 33 66 99 82.
[2] Tel.: +55 85 3366 90 08; fax: +55 85 3366 90 08.
[3] Tel.: +55 71 81430580; fax: +55 71 81430580.

0926-860X/$ – see front matter © 2009 Elsevier B.V. All rights reserved.
doi:10.1016/j.apcata.2009.02.036

W, Si, or Zn oxides have been tested as additives, and spinel oxides and various mixed oxides have been tested as catalysts or catalyst supports for the reaction [3,13–19]. Among these, spinel oxides have been screened extensively due to their benefits in preventing the deactivation process and increasing the activity of CO_2 dehydrogenation of ethylbenzene [9,16–20]. Nevertheless, the main reasons for the deactivation of these catalysts during the reaction are coking, loss of active components, the reduction of the promoters, and physical degradation of the solid [16,18].

In a previous experiment [21], the physico-chemical properties of MAl_2O_4 (where M = Cu, Ni, or both) were intensively studied. For the considerations of this paper, MAl_2O_4 is a stable system that possesses active sites of high activity and the lowest reducibility for transformations of hydrocarbons. These properties could be related to the following factors: (i) Al_2O_4 may stabilize the catalyst and thus prevent sintering; (ii) transition metals (Ni, Cu) are active components and increase the activity of the reaction; (iii) alkaline metals, *e.g.,* sodium, act as promoters and increase the activity and selectivity of the MAl_2O_4 catalyst.

In order to provide a deeper understanding of the catalytic performance of MAl_2O_4 and to investigate the possible causes of its deactivation, this work aims at examining the relationships between surface activities and structural features of the catalysts during its deactivation. These relationships were used to determine the causes of deactivation of the MAl_2O_4 system during styrene production by means of dehydrogenation of ethylbenzene with CO_2.

2. Experimental

2.1. Catalyst preparation

The catalysts studied in this work consisted of the spinel oxides NA, CA, and CAN referred to as nickel aluminate, copper aluminate, and mixed copper and nickel aluminate, respectively. Pure N and C samples are referred to as nickel and copper oxides, respectively.

The samples were prepared by a co-precipitation method at pH 11, using diluted metal precursor salts. The concentrations of all the solutions were 1 mol L^{-1}. In this synthetic procedure, a mixture consisting of 10% aqueous nitrate solutions containing Al^{3+} and Ni^{2+} (Reagen, $Al(NO_3)_3{\cdot}9H_2O$, 99 wt% and $Ni(NO_3)_2{\cdot}6H_2O$, 99 wt%) was slowly added, by means of a peristaltic pump, to a 5% sodium hydroxide solution (Reagen, NaOH, 98 wt%) in a beaker under vigorous stirring. The colloidal mixture was submitted to an aging treatment at 60 °C. The resulting gel was filtered and washed several times with de-ionized water until the pH reached 7 to remove the excess of sodium. Afterwards, the solid was dried and calcined in an air flow at 800 °C for 6 h to obtain NA.

CA was prepared by the above-mentioned route, mixing stoichiometric amounts of Al^{3+} and Cu^{2+} nitrates (Reagen, $Al(NO_3)_3{\cdot}9H_2O$, 99 wt% and $Cu(NO_3)_2{\cdot}6H_2O$, 99 wt%). In the case of the CAN ternary system, Al^{3+}, Cu^{2+} and Ni^{2+} nitrates were co-precipitated simultaneously, following the same method. N and C samples were synthesized by using only nickel and copper nitrates with sodium hydroxide, adopting the aforementioned methodology.

The overall chemical compositions of the solids are given in Table 1.

2.2. Catalytic experiments

Dehydrogenation of ethylbenzene with carbon dioxide was carried out in a tubular stainless steel reactor, where 0.1 g of catalyst was loaded per run. Before the catalytic measurements, the catalysts were activated *in situ*, under a nitrogen flow, from room temperature up to 550 °C over the course of 1 h. Thereafter, ethylbenzene (Fluka, 99.99 wt%) was fed through a vaporizer, where the nitrogen flow mentioned above was mixed with carbon dioxide (AGA 99.99 wt%) (molar ratio CO_2/EB = 30). The gas phase composition of the feed is nitrogen (11.73 mmol h^{-1}), carbon dioxide (58.69 mmol h^{-1}) and ethylbenzene (1.98 mmol h^{-1}). The mixture was then passed through the reactor continuously. The reaction was operated at atmospheric pressure, in the range of 530–610 °C. The products of the reaction were condensed in an ice/water trap and analyzed by a gas chromatograph (Simple Chrom model), which was equipped with a flame ionization detector. The gaseous effluents (H_2, CO_2 and CO) were analyzed in a thermal conductivity gas detector chromatograph (Ciola model). Blank runs demonstrated that ethylbenzene conversion was negligible.

Experimental conditions were varied as follows:

(a) For fresh catalysts, a temperature of 550 °C, a 6 h reaction time, and a CO_2/EB molar ratios of 9, 15 or 30;
(b) For fresh catalysts, a temperature of 550 °C, a 24 h reaction time and a CO_2/EB molar ratio of 9;
(c) For spent catalysts, recycling experiments were carried out to investigate the ability to regenerate the solids. The recycle of spent catalysts (submitted to condition b) was by heating the solids in air flow at 550 °C for 1 h to burn off the carbonaceous deposits;
(d) For reused catalyst, a CO_2/EB molar ratio of 30, a temperature at 550 °C, and a 6 h reaction time.

Results from a reproduced experiment showed that conversion and selectivity had an error of ±3%. Activities were calculated as the conversion of ethylbenzene per gram of catalyst per hour, while selectivities were calculated as the amount of desired products relative to total products formed.

Table 1
Chemical analysis of the MAl_2O_4 catalysts.

Sample	(wt%) Ni		(wt%) Cu		(wt%) Al	
	Theo	Exp	Theo	Exp	Theo	Exp
N	78.57	78.04	–	–	–	–
C	–	–	79.88	78.82	–	–
NA	33.33	32.91	–	–	30.56	31.27
CA	–	–	35.02	34.88	29.74	29.20
CAN	24.43	23.93	26.45	27.15	22.48	21.79

M^{2+}:Al^{3+} atomic ratio of 1:2.

2.3. Characterization of catalysts

The fresh, spent, and reused catalysts were characterized by various techniques.

Inductively coupled plasma optical emission spectroscopy (ICP-OES) was used to measure the concentration of nickel, copper, aluminum, or sodium in each of the samples synthesized above. The fresh catalysts were dissolved in a mixture of HNO_3 and HCl acids prior to the measurements. The obtained solutions were then analyzed in Varian equipment.

Surface areas and pore volume were determined by nitrogen adsorption–desorption analysis, which was performed on an Asap 2000 instrument. The fresh and spent samples were pretreated overnight at 250 °C under a vacuum of 5×10^{-3} torr. Specific surface areas were calculated using the BET equation.

X-ray diffraction (XRD) experiments were carried out on a Rigaku X-ray diffractometer (Rigaku model, 40 kV and 25 mA) using Cu Kα radiation. Crystal structures were determined using wide-angle diffraction patterns in the 2θ = 3–80° range. Reference patterns from ICDD (International Centre for Diffraction Data) were used for identification of bulk phases. The average size of the

particles, as well as the relative amount of the phases was determinated from the XRD data.

The infrared spectra of spent catalysts were obtained by a Perkin Elmer FTIR spectrometer in the range of 500–4000 cm^{-1}. One milligram of each sample powder was diluted with 200 mg of vacuum-dried IR grade KBr and submitted to a pressure of 8 tonnes.

A Philips XL-30 scanning electron microscope (SEM) was used to characterize fresh and spent catalysts. Elemental analysis was performed by energy dispersion using an EDX Link Analytical QX-2000 system coupled to the SEM microscope. For TEM image, a JEOM-12 1200EX electron microscope was used. The samples were ground and dispersed ultrasonically in acetone, and a drop of the suspension was then evaporated on a carbon-coated copper grid.

X-ray photoelectron spectra (XPS) of fresh, spent, and reused catalysts were recorded with a XPS Escalab MKII and VG apparatus, using AlKα radiation. The base pressure was 10^{-8} mbar. The binding energies (BE) were calibrated by using C1s peak of contaminant carbon (BE = 284.8 eV). BE of Al 2p, Ni $2p_{3/2}$ and Cu 2p core-levels, respectively at 73.8 eV, 855.5 eV and 932.0–935.0 eV were recorded.

Raman spectra of the spent catalysts were obtained on the T64000 Raman spectrometer (Jobin Yvon triple spectrometer) under ambient conditions. A 514.5 nm Ar laser was used as the exciting source with a power density of 1 MW cm^{-2} on the sample surface and a power of 120 mW. The measurements were referenced to Si at 521 cm^{-1} with 16 data acquisitions in 180 s.

The particle size (L) of spent catalysts was calculated from Raman intensity using the following equation [22,23]:

$$L(\mathrm{nm}) = \frac{560(I_D/I_G)^{-1}}{E_\lambda^4}, \quad \text{(I)}$$

in which λ = 514.5 nm and E = 2.41 eV; I_D and I_G are, respectively, the intensities of the D and G bands.

The temperature of reduction was obtained via TPR analysis from 25 to 1000 °C at a heating rate of 10 °C min^{-1}. N_2 gas containing 5% H_2 was used to reduce catalysts with a flow rate of 10 cm^3 min^{-1} for 0.35 g of fresh catalyst, using the Micromeritcs TPR/TPD 2900.

TGA experiments on spent catalysts were carried out in a Shimatzu TG/DTA 50 instrument to analyze the reduction in mass as a result of carbon oxidation. The measurements were performed from room temperature to 1000 °C at 10 °C min^{-1} under air flow. To analyze the gases formed after regenerating the $NiAl_2O_4$ spent catalyst and to identify the recycling ability *ex situ* of this catalyst, simultaneous TGA and DSC experiments were carried out using a Netzsch STA 409 PC/PG equipment coupled to a Bruker Tensor 27 IR instrument. The measurements were performed from room temperature to 1000 °C at 10 °C min^{-1} under air flow by placing approximately 15 mg of the sample in an aluminum pan.

Elemental analysis of carbon was performed in a Leco instrument on spent and reused catalysts to measure the concentration of carbon after the catalytic test.

3. Results and discussion

3.1. Specific characterization of fresh catalysts

The results of the chemical analysis of the catalysts show that experimental and theoretical values of copper, nickel, and aluminum are in agreement (Table 1). Indeed, the sodium concentration is less than 1% for all of the studied catalysts.

3.1.1. XRD and textural features of fresh samples

Fig. 1 displays the powder X-ray diffraction patterns of the fresh catalysts.

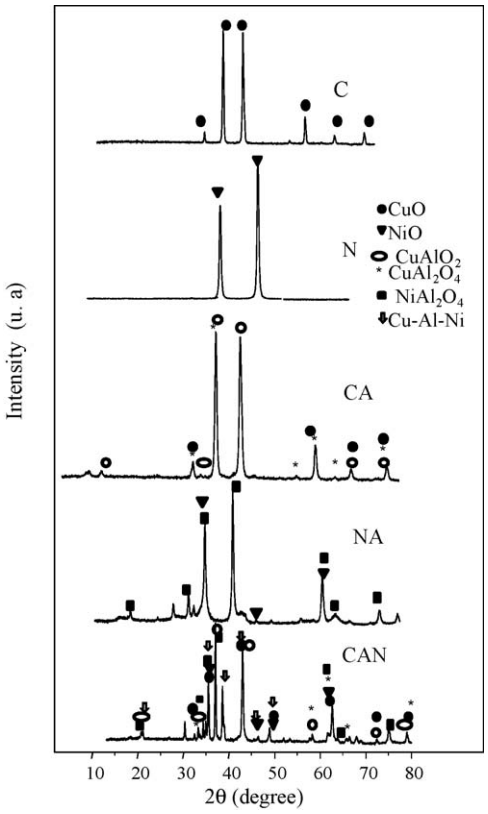

Fig. 1. XRD patterns of the fresh catalysts.

These patterns reveal that in the case of the N sample, cubic NiO is the only phase observed at the diffraction lines (1 1 1) and (2 0 0), whereas the C sample has a CuO crystalline phase at (1 1 0), (0 0 2), (1 1 1), (2 0 2), (0 2 0), and (2 2 0). The sharpness of the XRD peaks indicates the higher crystallinity of both solids, in which phases were identified by comparison with International Centre for Diffraction Data—ICDD (CuO, PDF n° 80-1268; NiO PDF n° 78-0423).

XRD peaks of spinel oxides are also shown in Fig. 1. The components of the CA sample were found to be CuO, $CuAlO_2$ (ICDD, PDF n° 39–0246), and $CuAl_2O_4$ (ICDD, PDF n° 78-1605); with the delafossite ($CuAlO_2$) and copper oxide (CuO) being the main two contributors. Table 2 summarizes the phases detected by XRD.

Considering the fact that the preparation of the CA sample is based on the co-precipitation method by controlling the nucleation and growth process, these phases are likely formed. Additionally, the formation of $CuAlO_2$ is favorable, according to DTA/TG studies [24] that suggest the following sequence of solid state reactions:

$$CuO + Al_2O_3 \rightarrow CuAl_2O_4 \quad (1)$$

$$CuAl_2O_4 + CuO \rightarrow 2CuAlO_2 + 1/2O_2 \quad (2)$$

For the NA sample, NiO and predominantly $NiAl_2O_4$ (ICDD, PDF n° 71-0963) are detected. The reactions that represent the formation of the referred phases are described as follows [25]:

$$2NiOOH \rightarrow 2NiO + H_2O + 1/2O_2 \quad (3)$$

$$2NiO + 1/2O_2 \rightarrow Ni_2O_3 \quad (4)$$

$$NiO + Al_2O_3 \rightarrow NiAl_2O_4 \quad (5)$$

Reactions 3–5 explain the predominance of 74.2% of $NiAl_2O_4$ spinel structure in the NA sample, as determinated by XRD data.

Table 2
Characteristics of the catalysts studied.

Sample	Phases detected[a]	BET surface area ($m^2\ g^{-1}$) [b]	Particle size[a] (nm)	Reduction temperature[c]
N	NiO	23	16.8	405;530
C	CuO	17	17.4	310
NA	(74.2%)$NiAl_2O_4$ + (28.8%) NiO	26	22.8	221; 402
CA	(51.6%)$CuAlO_2$ + (15.0%) CuO + (33.3%) $CuAl_2O_4$	57	15.5	200–289; 289–609; >609
CAN	(18.1%)Cu-Al-Ni + (12.4%)CuO + (14.1%)$CuAlO_2$ + (3.2%)Cu_2O + (26.7%)$NiAl_2O_4$ + (9.5%)NiO + (16.2%) $CuAl_2O_4$	10	30.7	424; 200–800; >804

[a] From XRD experiments.
[b] Data obtained from N_2 adsorption–desorption analyses.
[c] From TPR experiments.

The CAN sample has the spinel phases $NiAl_2O_4$ (26.7%), $CuAl_2O_4$ (16.2%), and $CuAlO_2$ (14.1%), with the latter coexisting with CuO (15.4%). Nickel oxide (9.5%) is also observed. Interestingly, peaks at 2θ = 21,0; 35,4; 38,7; 43,4; 46,2; 48,8 that correspond to hkl planes (1 1 0), (0 2 2), (1 2 2), (0 0 1 8), (1 2 8), and (2 0 8) are assignable to a ternary Cu-Al-Ni spinel system denoted as martensite. This spinel structure is an alloy commonly used in metallurgy and as a semiconductor [26,27].

The structure of MAl_2O_4 (where M = Cu^{2+}or Ni^{2+}) is known to be almost an inverse spinel, with the M^{2+} ions preferentially distributed over the octahedral cation sites (A-site) in a AB_2O_4 binary spinel structure. The effect of substitution of Cu^{2+} for Ni^{2+} and vice-versa in an aluminate matrix generates a competition. Accordingly, Cu^{2+} cations can gradually replace Al^{3+} in B-sites of aluminate and occupy at the same time the vacant A-site to compensate the charge balance. Another possibility is to replace Al^{3+} ions by Ni^{2+}. Also, as the Cu^{2+} ion has a larger radius than Ni^{2+}, the occupation of vacant sites with Cu^{2+}causes the expansion of the spinel lattice. Indeed, both Ni^{2+} and Cu^{2+} can coexist with aluminum forming the Cu-Al-Ni martensite structure.

All of the above possibilities were considered to explain the formation of the phases in the CAN sample. In addition, based upon the XRD patterns using Scherer's equation, the sizes of the particles were found to be between 15.5 nm and 30.7 nm (Table 2).

Table 2 also demonstrates that CA and NA have the highest surface areas, while CAN has the lowest. This can be explained by the fact that the various oxides formed coexist in the CAN sample, as seen by XRD and further confirmed by SEM–EDX and XPS experiments. Also, the largest particle size, *e.g.,* 30.7 nm, is consistent with the lowest value of the BET surface area of this sample. Thus, the surface area of CAN ($10\ m^2\ g^{-1}$) decreases drastically, as compared to the analogous CA and NA samples (57 and 26 $m^2\ g^{-1}$, respectively). Comparing the latter samples, it can be noted that bulk $NiAl_2O_4$ particles (22.8 nm) decrease the textural parameter of the nickel aluminate as compared to one of the $CuAl_2O_4$ parent spinel oxides (15.5 nm). N and C catalysts have intermediate surface area values as shown by the values of the oxides obtained by the same preparation method [23].

3.1.2. SEM images of fresh catalysts

The morphology of the obtained spinel oxide materials was observed by SEM and is shown in Fig. 2.

The NA sample exhibits an irregular rough plate-like morphology with disordered grains that are mainly attributed to nickel species (Fig. 2a). The EDX analysis of different particles suggests a distribution of nickel in the aluminate structure.

The SEM image of CA is given in Fig. 2b. This solid is made up of aggregates of spherical particles. EDX results show that the

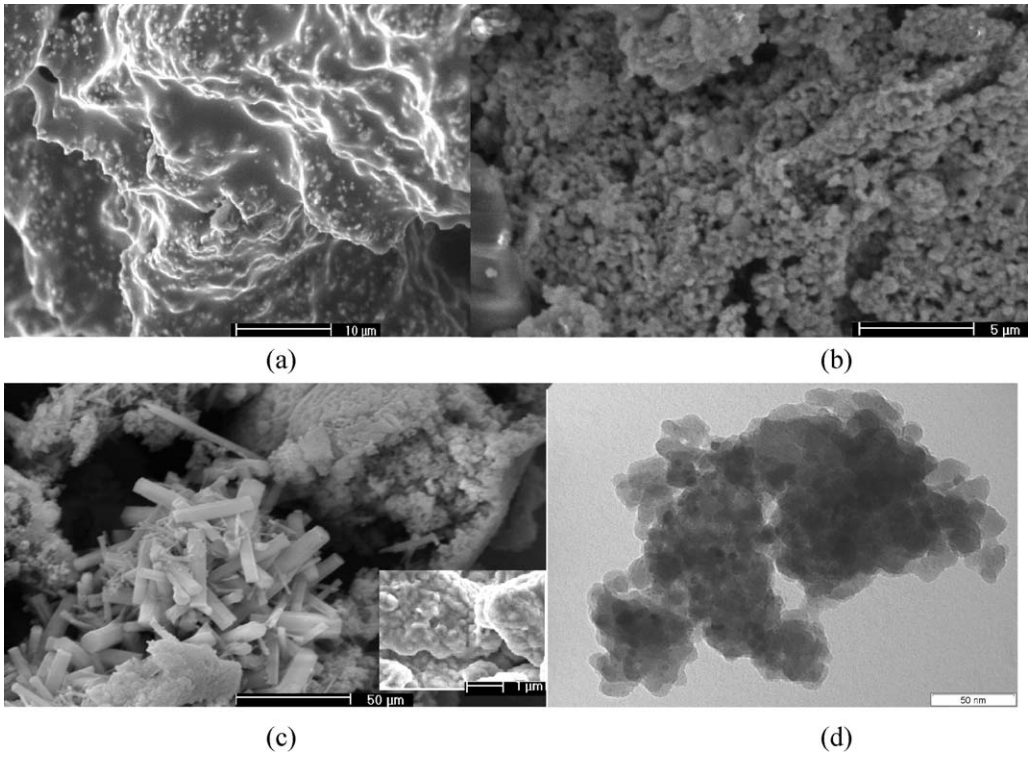

Fig. 2. SEM images of the fresh catalysts: (a) NA, (b) CA, (c) CAN. TEM image of CAN sample (d).

concentration of copper species at the surface of the fresh catalyst is somewhat higher than in the bulk.

The SEM micrograph of the CAN sample (Fig. 2c) is composed of disordered particles of spherical morphology that coexist with other particles in various configurations. A higher magnification reveals a non-uniform sphere-like particle (see inset in Fig. 2c). Thereby, the various oxides observed by XRD can be present in this sample. Interestingly, EDX analysis demonstrates that the nickel and aluminum contents of the large spherical aggregates are much higher than the surrounding particles, in which the copper concentration is essentially constant. This discontinuity in copper, nickel, and aluminum concentrations suggests that the thermal treatment at 800 °C results in a segregation of phases in the CAN sample. Indeed, the TEM image of CAN sample (Fig. 2d) shows the agglomeration of particles with irregular morphology, with diameter around 5–35 nm. We have further used XPS analysis to obtain information about the nature of these phases formed on solid surface.

3.1.3. XPS studies

The XPS technique is much more sensitive than XRD for the detection of the positions of surface oxides. The obtained results are helpful in identifying the positions of M^{2+} ions in MAl_2O_4 catalysts.

For the samples, Al 2p and O 1s are observed at BE = 73.8 eV and in the 529.8–530.6 eV range. BE of Ni 2p and Cu 2p core-levels were recorded at 855.5–856.2 eV and 932.6–935.0 eV, respectively (Table 3).

For N and C samples, BE at 855.5 eV and 933.8 eV can be attributed to $Ni^{2+}$and Cu^{2+} species [28–30], respectively. This confirms the previous results of XRD that detected the sole presence of nickel and copper oxides in these samples.

In the case of the NA sample, only Ni^{2+} was found on the surface. There are no signals that can be attributed to the lattice oxygen of NiO that has a BE of 530 eV; this suggests that the Ni^{2+} ions are mostly incorporated into the framework of $NiAl_2O_4$ (BE = 856.2 eV) [28], as also suggested by SEM–EDX results.

The CA sample exhibits BE for Cu^{2+} and Cu^{1+} at 933.8–935.0 eV and 932.7 eV [30], respectively, with Cu^{1+} being the major component. This indicates that copper is present in $CuAl_2O_4$, CuO, Cu_2O phases; $CuAlO_2$ is the main phase on the surface of CA sample. This coincides with SEM–EDX and XRD data.

For the CAN sample, BE of 73.8 eV, 932.7–935.0 eV, and 855.5 eV were detected and suggest the simultaneous presence of Al^{3+}, Cu^{2+}, Cu^{1+}, and Ni^{2+} ions, respectively, on the solid surface. The values of percentage mass of surface atomic ratio are also given in Table 3.

The nickel concentration on the surface of NA is approximately 2%, confirming that most of Ni^{2+} ions are in the solid framework, as a $NiAl_2O_4$ phase (BE = 856.2 eV). The copper atomic ratio of the CA sample is 12.6%; with Cu being present mostly as Cu^{1+} (BE = 932.6 eV). A BE of 935.0 eV was also found and it indicates

Table 3
Binding energy (BE) and surface atomic ratio (% mass) data of the fresh catalysts.

Sample	BE (eV)				Percentage		
	Cu^{2+}	Cu^{1+}	Ni^{2+}	Al^{3+}	Cu^{2+}	Cu^{1+}	Ni^{2+}
N	–	–	855.5	–	–	–	0.5
C	933.8	–	–	–	0.2	–	–
CA	935.0 933.8	932.7 932.6	–	73.8	5.2	7.4	–
NA	–	–	855.5 856.2	73.8	–	–	2.3
CAN	935.0 933.7	932.7	855.5 856.2	73.8	3.0	8.5	7.7

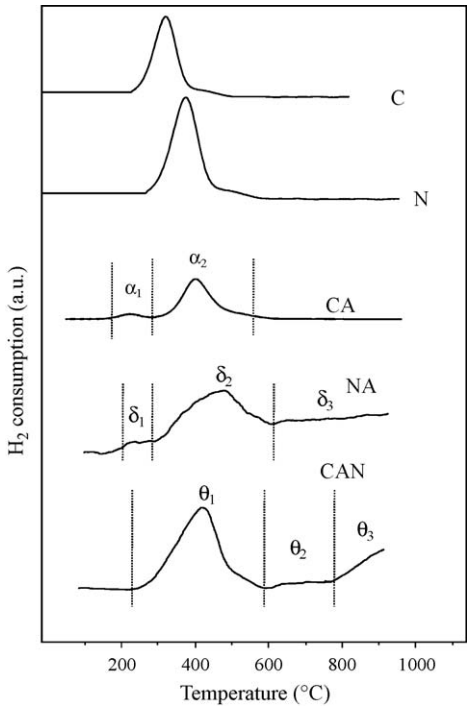

Fig. 3. TPR analyses of the solids.

the formation of $CuAl_2O_4$ phase. In the case of the CAN sample, the predominance of Cu^{1+} (8.5%) and Ni^{2+} (7.7%) confirms the existence of Cu_2O, NiO, and $NiAl_2O_4$ on the surface. The presence of these phases contributes to the decrease of the textural parameter values of the CAN sample.

3.1.4. TPR analysis

Temperature-programmed reduction (TPR) profiles of the solids are shown in Fig. 3.

The TPR curve of the N sample displays a two-step reduction of nickel: the first step has high intensity (at 405 °C), and the second one displays a flat peak at 510 °C. These steps are related to the reduction of nickel, which occurs according to the following reactions [31]:

$$NiO_X + nH_2 \rightarrow NiO + nH_2O \quad (6)$$

$$NiO + H_2 \rightarrow Ni + H_2O \quad (7)$$

Indeed, the small peak of reduction can be formed due to the reduction of some nickel species, which are obtained at high temperatures of calcination.

By contrast, C presents only one peak at approximately 310 °C, which is characteristic of the reduction of highly dispersed CuO [32].

The H_2-TPR profiles of spinel oxides show major differences from the pure metal oxides. The CA sample shows two distinct peaks at 221 °C and 402 °C, labeled α_1 and α_2, which correspond to the reduction of highly dispersed CuO and spinel $CuAlO_2$ [31,32], respectively (Table 2). The high temperature of the second peak indicates the difficulty of reducing Cu^{2+} in both the $CuAlO_2$ and $CuAl_2O_4$ phases.

NA curve shows three reduction steps, designated as δ_1 (200–289 °C), δ_2 (289–609 °C) and δ_3 (>609 °C). These peaks are attributed to reactions 6 and 7 and to hard reduction of $NiAl_2O_4$, respectively. CAN also has three reduction steps: θ_1 (at 424 °C), θ_2 (600–800 °C) and θ_3 (>804 °C). The TPR θ_1 stage can be influenced by the ease of reduction of NiO, Cu_2O and CuO species on the external surface of the solid, in regard to the peaks of the N and C

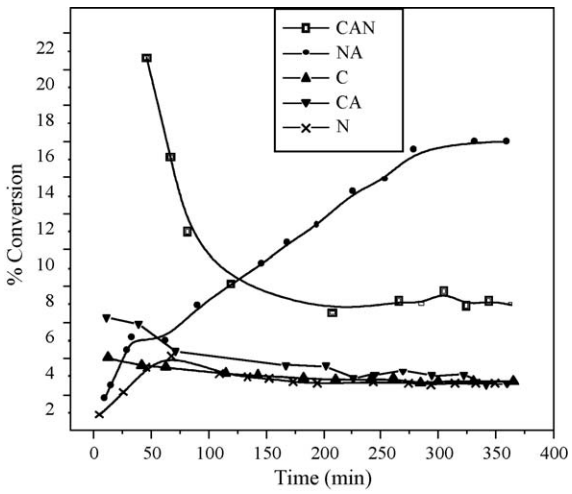

Fig. 4. Ethylbenzene conversion (% mol) vs. reaction time for all catalysts. Reaction conditions: catalyst: 100 mg; N_2: 11.7 mmol h^{-1}; CO_2: 58 mmol h^{-1}; EB: 1.98 mmol h^{-1}(CO_2/EB ratio = 30); T = 550 °C.

samples and XPS results. The θ_2 stage is associated with $CuAlO_2$, $CuAl_2O_4$ or $NiAl_2O_4$ reduction. Further increase to the θ_3 stage is caused by the increasingly difficult reduction of the martensite Cu-Al-Ni ternary system. Because of the size of the particle, the reduction peak becomes larger, and the martensite phase is reduced at temperatures upward of 800 °C.

Concerning the temperature of reduction, these data demonstrate that reduction of CAN and NA is difficult in comparison with the other samples. This behavior is particularly interesting because it provides conclusive evidence that the temperature (800 °C) is not high enough to reduce all the transitions metals. Therefore, the temperature of reduction increases, mainly for CAN, in which a highly stable martensite phase (Cu-Al-Ni) and $NiAl_2O_4$ are present.

3.2. Catalytic activity in the dehydrogenation of ethylbenzene with CO_2

Fig. 4 shows the overall ethylbenzene conversion, defined as the fraction of ethylbenzene reacted after a given reaction time for the different catalysts studied in this work, at 550 °C and a CO_2/EB molar ratio of 30.

At short reaction times, CAN shows high conversion (21%), while the other catalysts have conversion levels below 6%. When the reaction time increases, CAN exhibits a drop in the catalytic performance, reaching only about 7% conversion after 6 h of reaction; over a NA sample, 16% conversion is achieved after the same reaction time. This differs from the other samples, which reach 4% conversion after the catalytic run.

Comparison of the catalysts behavior is very interesting, as seen. Initially, all copper-containing catalysts are active (*e.g.* CAN, CA and C samples); it seems that Cu^{2+} and Cu^{1+} species found over these solids are catalytically active in the dehydrogenation of ethylbenzene with CO_2.

The initial conversion of the CAN catalyst is the highest, as compared with its Cu-containing counterparts. However, the conversion steeply decreases over all these catalysts. Studies on copper aluminates [33–36] in reactions involving ethylbenzene, as well as CO and CO_2, have revealed that the Cu^{2+} and Cu^{1+} species on the surface of catalysts generate the activity, but these species are not stable under dehydrogenation or CO oxidation conditions due to the reduction of Cu^{2+}/Cu^{1+} to Cu^0 species (further observed by XRD and XPS) at the beginning of the reaction.

In addition, conversion over a CAN catalyst decreases faster than over other solids, probably due to its low surface area (10 m^2 g^{-1}) and thus a lesser surface availability of the active phase. Moreover, on the CAN catalyst, ethylbenzene conversion decreases upon increasing the time on stream to attain high activity, when compared to its Cu-containing catalyst analogues. From this observation, it may be concluded that other phases (*e.g.,* Cu-Al-Ni and $NiAl_2O_4$) besides the one of copper lead to higher conversion and stabilization of the solid.

The Ni-containing catalyst behaves similarly, with an increase of the ethylbenzene conversion over time. In this case, the presence of a Ni^{2+} oxidation state provides a significant catalytic conversion. Nevertheless, the increase of the NA conversion with time on the stream indicates that the existence of Ni^{2+} as a NiO specie is not enough to maintain the conversion and thus that the $NiAl_2O_4$ bulk phase governs the conversion of ethylbenzene, as observed in previous studies [28,33].

Additionally, there is no clear correlation between the catalytic activity and the textural properties of the solids; for instance, the catalysts possessing the highest BET surface area (*e.g.,* CA sample, 57 m^2 g^{-1}) have a modest catalytic performance, while the one with the lowest value of textural parameters (*e.g.,* CAN sample, 10 m^2 g^{-1}) shows a better activity. On the contrary, intermediate values of the BET surface area (*e.g.*, NA sample 27 m^2 g^{-1}) display high conversion. Therefore, the textural properties appear to be a mere additional factor when considering the relevance of the active species formed on the catalysts. This implies that the reduction of the active phases of the catalysts (shown by TPR analysis, Table 2) significantly influences the catalyst conversion.

As the catalytic activity during the dehydrogenation of ethylbenzene is related to the low reducibility of the catalyst [19], it may explain the high performance of CAN. However, other factors besides reducibility can explain the activity of the NA sample. According to the reaction mechanism, simple dehydrogenation of ethylbenzene to styrene (reaction (8)) can take place over spinel oxides:

$$C_6H_5CH_2{-}CH_3 \rightarrow H_2 + C_6H_5CH{=}CH_2 \quad (8)$$

If CO_2 is co-fed in the reaction, the rate of H_2 production decreases, while the rates of CO and H_2O increase. This suggests an improvement of the ethylbenzene production by combining reaction (8) with the reverse water–gas shift reaction, RWGS (reaction (9)).

$$CO_2 + H_2 \rightarrow CO + H_2O \quad (9)$$

Consequently, the dehydrogenation equilibrium is shifted towards products under a CO_2 atmosphere. This was further confirmed by flowing 1.520 mmol h^{-1} of CO_2 with 0.0432 mmol h^{-1} of H_2 over a CAN sample. The amount of H_2 produced (0.0217 mmol h^{-1}) is approximately the same as the one of CO (0.0213 mmol h^{-1}), confirming that reaction (9) takes place. Hydrogen alone, as well as the products of the reaction (9) can be responsible for the reduction of the NiO, CuO, Cu_2O and $CuAlO_2$ phases that are easily reduced, as shown by TPR experiments. These data demonstrate the close relationship between ethylbenzene dehydrogenation and CO_2 hydrogenation.

As CAN sample is composed of a highly stable ternary system in which the Cu-Al-Ni phase is stable, the reduction of the other reducible phases is completed while Cu-Al-Ni can be maintained at a higher oxidation state during the reaction. This can explain the better performance of this solid in comparison with the others. Although NA shows a higher ethylbenzene conversion, it does not exhibit the same trend as CAN in terms of reducibility. Thus, it can be supposed that $NiAl_2O_4$ is an active phase that retains the surface nickel species at a high oxidation state because an excess of CO_2 is used during the reaction.

Table 4
Activities (a) and selectivities to styrene (S_{St}), toluene (S_T), benzene (S_B) and unidentified product (S_X) studied at different temperatures. Activities and selectivities were measured in mol g^{-1} h^{-1} and molar percentage, respectively.

Temperature	NA					CA					CAN				
	$a \times 10^3$	S_{St}	S_T	S_B	S_X	$a \times 10^3$	S_{St}	S_T	S_B	S_X	$a \times 10^3$	S_{St}	S_T	S_B	S_X
610	86.8	10.6	80.4	2.9	5.3	14.3	55.7	15.0	25.9	2.7	37.3	17.4	74.3	4.2	3.7
580	49.4	31.8	60.7	2.8	4.4	8.1	64.3	14.6	20.5	0.2	15.1	30.3	52.4	15.2	2.0
550	16.0	90.7	3.2	2.8	1.0	2.3	75.2	7.1	16.7	0.8	4.0	21.8	63.8	13.6	0.8
530	2.2	97.3	1.2	1.4	0.1	1.0	84.6	1.3	14.1	0.2	1.6	38.2	43.5	17.1	1.2

Spinel oxides containing nickel or copper as active components are well known for promoting dehydrogenation of ethylbenzene to styrene using steam [17]. Therefore, these active components could be efficient for styrene production via dehydrogenation of ethylbenzene, with CO_2 as a co-reagent. During the reaction, the defect formed by the lattice oxygen uptake can be refilled by oxygen from CO_2 gas, resulting in no substantial change in the structure of the solid under a CO_2 atmosphere. It appears that ethylbenzene dehydrogenation over $NiAl_2O_4$ phase occurs at the redox sites on the surface of the solid, and CO_2 behaves as an oxidant for Ni species. These species are kept at a high oxidation state with CO_2 during the reaction.

Despite the fact that CO_2 is an oxidant, even a larger amount of CO_2 (CO_2/EB = 30) is not enough to act as a mild oxidant agent to avoid the reduction of the NiO, CuO and $CuAlO_2$ phases. Thus, the results demonstrate that the referenced active components are easily reduced. In contrast, the Cu-Al-Ni phase in CAN is less reduced due to the electronic properties of donating electrons from Cu to Ni, by avoiding the reduction of Ni in an aluminate matrix [33]. NA sample having $NiAl_2O_4$ phase exhibits a much higher activity, most likely due to the presence of CO_2, which avoids the loss of the active Ni^{2+} component. These facts may explain the performance of the $NiAl_2O_4$ and Cu-Al-Ni phases in comparison with the other materials.

Fig. 5 shows the distribution of the products of each catalytic system. The products formed over the catalysts were analyzed at comparable ethylbenzene conversions, running near steady state conditions. It is worth noting that the same types of products, including styrene and benzene, are obtained over all catalysts. Over NA and CAN, toluene is also formed. An inspection of the light products reveals that ethane, methane, hydrogen and carbon monoxide are also formed.

Since the conversion levels using N, C and CA are too low, the levels of products formed over these samples are negligible. Among the catalysts investigated, NA gives higher styrene production than CAN (respectively, 90 and 30%), the latter being highly selective to toluene. This behavior is not well understood and deserves further investigation.

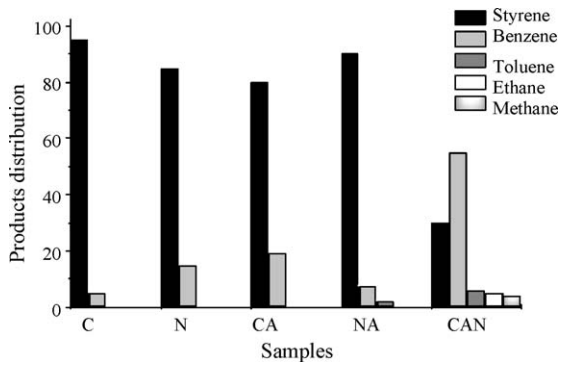

Fig. 5. Distribution of the products obtained. Reaction conditions: catalyst: 100 mg; N_2: 11.7 mmol h^{-1}; CO_2: 58 mmol h^{-1}; EB: 1.98 mmol h^{-1}(CO_2/EB ratio = 30); T = 550 °C.

3.2.1. Effect of temperature on the catalytic performance

By thermodynamics calculations, Sun et al. [15] have shown that there is a dependence of the equilibrium conversions of ethylbenzene and CO_2 for the dehydrogenation of ethylbenzene in the presence of CO_2. This is confirmed in the present study as the calculated equilibrium conversions are 50.2, 67.3, 85.4, and 92.2% at 530, 550, 580 and 610 °C, respectively. The ethylbenzene activity and selectivity were obtained at different temperatures with a CO_2/EB ratio of 30 (Table 4).

The steady state values of activity reveal that catalytic activity increases with increasing temperature for all catalysts investigated, in accordance with thermodynamic principles. Both N and C present low conversion (below 5%), even if the temperature is raised; therefore, the activities over these catalysts were not evaluated at different temperatures. Furthermore, the absence of spinel phases over the N and C samples destabilizes these oxides. Consequently, they are easily reduced during the reaction, as suggested by the TPR results and further confirmed by XPS of spent catalysts.

Moreover, the selectivity to styrene has a reverse trend as the temperature increases; for instance, selectivity to styrene gradually decreases from 97.3% at 530 °C to 10.6% at 610 °C, in the case of NA. In addition, thermal conversion of ethylbenzene cannot be neglected at high temperatures, and it can likely explain the high levels of toluene and benzene obtained. This indicates parallel ethylbenzene cracking and hydrogenolysis reactions, reactions (10) and (11), respectively:

$$C_6H_5CH_2{-}CH_3 \rightarrow C_2H_4 + C_6H_6 \quad (10)$$

$$C_6H_5CH_2{-}CH_3 + H_2 \rightarrow C_6H_5{-}CH_3 + CH_4 \quad (11)$$

Reactions (10) and (11) are confirmed by the large amounts of the byproducts of cracking of ethylbenzene at high temperatures, such as ethane and methane (S_x). Traces of gases consisting of carbon monoxide and hydrogen are also found. Low selectivities to styrene indicate that reactions (10) and (11) become important at high temperatures over NA and CAN. Indeed, over NA, the existence of high amounts of toluene, *e.g.*, >80.4% at higher temperatures suggests the predominance of hydrogenolysis (reaction (10)) over this solid. Styrene cracking at high temperatures also accounts for the decrease in the product selectivity by forming carbonaceous materials on the catalyst surface (reaction (12)) [4,9]. Reactions 10–12 contribute to the production of large amounts of byproducts at temperatures higher than 550 °C.

$$C_6H_5CH = CH_2 \rightarrow 2H_2 + \text{coke} \quad (12)$$

Styrene selectivity is much higher over CAN than over the other catalysts when increasing the temperature from 530 to 610 °C. This indicates copper selectivity to styrene at moderate temperatures, and it suggests that spinel structure of finely dispersed $CuAlO_2$ and $CuAl_2O_4$ strongly affects the catalyst selectivity.

Additionally, over NA, a significant gain in styrene selectivity is observed at moderate temperatures by promoting the solid with sodium due to inhibition of the reduction of nickel. Promoting $NiAl_2O_4$ with sodium does efficiently reduce the acidity of the surface [3–19], since byproducts formed on acidic sites, *e.g.*, toluene and benzene, are not obtained in any significant amount, in agreement with our results.

The crystalline growth of nickel particles was not avoided, particularly over NA, as observed further by the characterization of spent catalysts. As a consequence, carbon fouling, identified as the main cause of the loss of styrene selectivity, is slightly diminished. However, the byproduct amounts are not large enough to account for the decrease in styrene selectivity of $NiAl_2O_4$ phase of NA sample at lower temperatures.

It is well known that nickel aluminate is an inverse spinel, in which the Al^{3+} trivalent cations occupy all the tetrahedral sites while the octahedral ones are filled by half of the trivalent cations and all the Ni^{2+} divalent cations that have the electronic configuration $3d^8$ [34,38]. The ambient temperature controls whether the occupancy of Ni^{2+} will be in tetrahedral and octahedral sites. Therefore, Ni^{2+} ions, which occupy the tetrahedral site in a normal spinel, can move into the octahedral sites, while half of the Al^{3+} ions can move in an opposite direction to fill the states already occupied by Ni^{2+} ions.

Hence, the divalent cation is stabilized in an aluminate matrix, without any reduction to Ni^0, as confirmed by XPS analysis of fresh catalysts. On one hand, this favors an increase in the activity in highly reducible media. On the other hand, the selectivity is biased due to the extent of the movement of cations, which results in defects and forms isolated sites, both of which can favor carbonaceous filaments on nickel vacancy sites [28,29].

It is generally accepted [6,9,19] that dehydrogenation of ethylbenzene with a CO_2 mechanism must have a good balance between the acid and base sites in order to obtain high catalytic activity. According to these findings, the reaction occurs by the following the steps: first, the adsorption of ethylbenzene on the acid or base site; second, the abstraction of the α-hydrogen of ethylbenzene by a basic surface oxygen (adjacent to the acid site) located at defect sites, which may leave two free OH groups at the surface of the catalyst; third, the formation of an anion vacancy via desorption of water and the re-oxidation of the vacancy site by an O^- species formed from adsorbed CO_2; and last, the abstraction of the β-hydrogen from ethylbenzene by the O^- species in order to give styrene and an OH group. This possible mechanism was reported by Mars-van Krevelen for iron oxide catalysts [38]. Therefore, the mechanism of styrene production on NA can be explained by the considerations mentioned above.

In the case of the CA catalyst, selectivity to styrene is not reduced by increasing the temperature, in contrast with NA and CAN. This can be explained by the fact that the phases present on CA (*e.g.* $CuAlO_2$, Cu_2O, CuO and $CuAl_2O_4$) are easily reduced, and another reason is that copper particles do not enhance carbon deposition; however, Ni^0 particles can increase the amount of encapsulating carbon (deactivating), which is difficult to gasify by CO_2. This also contributes to a decrease in selectivity to styrene. However, CAN has the lowest styrene selectivity among the catalysts studied. The ternary system produces mainly toluene at high temperatures, probably as a result of condensation of styrene to form stilbene dimmers (diarylethene), which further decompose into two molecules of toluene:

$$2C_6H_5CH = CH_2 \rightarrow C_6H_5CH = CHC_6H_5 + C_2H_4 \rightarrow 2C_6H_5{-}CH_3 + 2C \quad (13)$$

The Cu-Ni alloy in the CAN sample could be responsible for an electron donation from Cu to the *d* orbital of Ni, which could explain the easier reducibility of Cu, as seen in many catalytic reactions [34,35]. However, the ternary system is composed of aluminum as well as nickel and copper (Cu-Al-Ni). Hence, the aforementioned metals are in an aluminate matrix, which avoids the reduction of the copper species. Therefore, the results suggest that CuO, Cu_2O, $CuAlO_2$, $CuAl_2O_4$ and NiO species become more reduced than the martensite (Cu-Al-Ni) phase, which is stabilized on the surface of CAN. In reality, the reduced phases can produce toluene, which is justified considering the decrease of styrene selectivity in CA. These results demonstrate that nickel stabilized in an aluminate matrix favors the formation of styrene if carbon deposition does not take place.

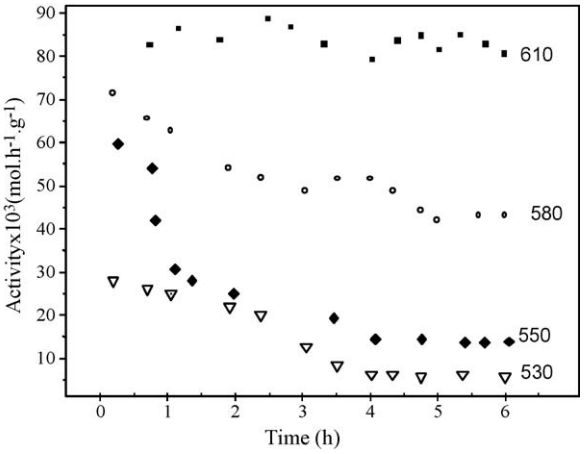

Fig. 6. Activity of ethylbenzene at different temperatures for NA sample at CO_2/EB = 30.

The higher values of styrene selectivity and yield obtained from NA led to an inspection of the catalyst activity versus time at different temperatures, as seen in Fig. 6.

A slight decrease in activity can be clearly observed at short reaction times, independent of temperature. As the reaction time increases, activity over NA is observed to stabilize at different levels, with the temperature at 550 °C a steady state condition where activity and selectivity are quite stable.

In summary, the activity of the catalysts in ethylbenzene conversion follows the order: NA > CAN > CA > N > C, while the selectivity to styrene has a slightly different order of: NA > CA > CAN, with N and C samples not evaluated because their conversion level is too low. Cu^{2+}, Cu^{1+} and mainly Ni^{2+} species are actives for the reaction.

Activities increased with increasing of temperature; conversely, selectivity to styrene has an opposite trend, especially at high reaction temperatures (≥550 °C). Indeed, the addition of Ni^{2+} in an aluminate matrix can avoid the reduction of metal, hinder coke formation and also sustain the stability of the catalyst.

3.3. Characterization of spent catalysts

In order to understand the origin of catalyst deactivation, we have characterized the spent catalysts by various techniques.

3.3.1. XRD and Raman results

The XRD patterns of the catalysts used in the reaction are shown in Fig. 7.

The XRD profiles of N and C samples are typical reduced Ni^0 and Cu^0 patterns. N possesses some peaks characteristic of stabilized Ni^{2+}, whereas the CA spent catalyst consists of a mixture of Cu^0 (42.8%) and CuO (14.2%). A 43% of $CuAl_2O_4$ can also be detected for the last sample. This indicates that the excess of carbon dioxide used during the reaction may play an important role in maintaining the oxidized species, and with it, the activity of the

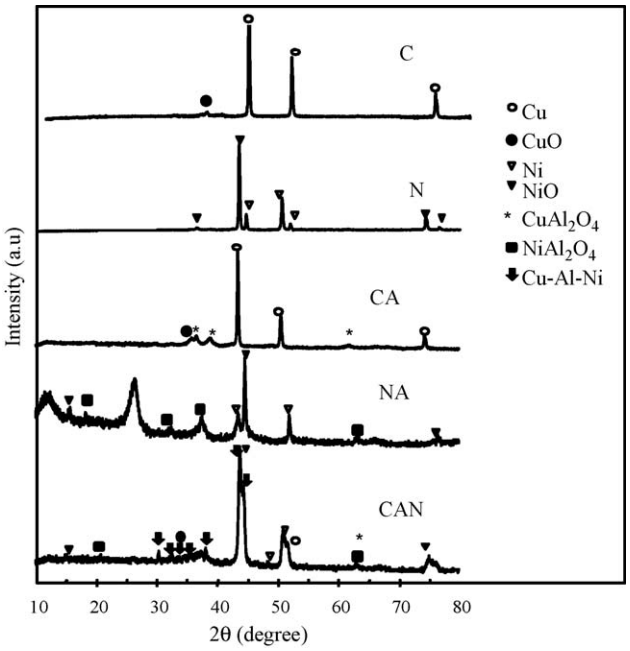

Fig. 7. XRD patterns of the spent catalysts after being used at 550 °C for 6 h of reaction at CO_2/EB = 30.

catalyst, as observed in various transition metal based catalysts [11,33,37].

These findings suggest that in copper aluminate solids, a thick $CuAl_2O_4$ layer is stabilized by bulk CuO [35] that prevents the reduction of $CuAl_2O_4$. However, Cu^{2+} ions are not the active species for ethylbenzene dehydrogenation [33], as demonstrated by the low conversion and selectivity obtained with this solid. Fig. 7 shows that the NA spent sample consists of a $NiAl_2O_4$ phase (44.4%). This is in accordance with [37]. Moreover, some peaks of NiO (22.2%) and Ni^0 (33.4%) clearly appear in the XRD patterns and indicate the physical degradation of the $NiAl_2O_4$ sample after the catalytic run. In addition, the peak at $2\theta = 25.5^\circ$ (0 0 2) corresponds to the inter-planar spacing, a characteristic of highly oriented pyrolytic graphite [39], that is further confirmed by Raman spectroscopy investigations.

As noted above, CO_2 stabilizes Ni^{2+} species in an aluminate, and hence the rate of reactions 8 and 9 is not enough to reduce nickel species. The results also show that $NiAl_2O_4$ is the active phase of the reaction, and the residual sodium is a promoter, which leads to the high catalytic activity and selectivity of the solid.

The diffraction peaks of spent CAN display the reduced phases, such as Cu^0 (2.8%) and Ni^0 (3.7%); also, $NiAl_2O_4$ (17.6%) and Cu-Al-Ni (41.2%) oxidized phases, as well as large amounts of CuO, NiO and $CuAl_2O_4$ (31% of the total amount) were found. This means that the major active component for the dehydrogenation of ethylbenzene with CO_2 is $NiAl_2O_4$ and justifies the activity of the CAN sample. This hypothesis was confirmed by studies on the copper and nickel catalysts obtained by the sol–gel method that demonstrated that there is a synergistic effect due to the co-existence of the NiO and CuO phases in the catalysts investigated for the oxidation of CO to CO_2 [23]. According to the authors, the possible redox couples involved in the catalytic CO oxidation are Cu^{2+}-Cu^{+1}, Cu^{1+}-Cu^0 and Ni^{3+}-Ni^{2+} according to reaction (14):

$$Ni^{2+} + Cu^{2+} \rightarrow Ni^{3+} + Cu^{+} \quad (14)$$

The trivalent nickel cations are active sites for chemisorption of CO, and the monovalent copper cations are involved in chemisorption of O_2 [23]. Therefore, we infer that the reverse reaction (14) can occur over CAN during dehydrogenation of ethylbenzene with CO_2. Cu^+ and Ni^{3+} pairs are probably responsible for the decrease of the reaction rate due to the shifting of the equilibrium of reaction (15) when the reaction takes place in a single step over CAN.

$$C_6H_5CH_2{-}CH_3 + CO_2 \rightarrow H_2 + C_6H_5CH = CH_2 + H_2O + CO \quad (15)$$

This hypothesis is supported by the activity of this solid in comparison with NA catalyst. The excess of CO_2 also contributes to maintain the CuO, NiO, Cu-Al-Ni, and $NiAl_2O_4$ phases, whereas Cu^0 and Ni^0 were found in small amounts, as shown by the XRD results. However, the presence of reduced copper and nickel species moderates the catalytic performance, as byproducts are favored instead of styrene, even when stable Cu-Al-Ni is present. Moreover, the black color of CAN suggests coke formation on the solid surface. Meanwhile, NA had a black color with pale-green points after the catalytic test, an indication that severe coke deposition (XRD peak at $2\theta = 25.5^\circ$) or reduction of the solid can occur. The last possibility is negligible, as indicated by the XRD results.

Raman spectroscopy is more sensitive at the surface region, while XRD gives information about both the surface and the bulk [39–41]. Fig. 8 shows Raman spectra of the spent catalysts investigated.

For CA, bands at 145, 194, 217, 293, 417, 629 and 847 cm^{-1} (Fig. 8a), are detected, corresponding to the bulk CuO [42]. Although XRD detected CuO, Cu and spinel $CuAl_2O_4$ over CA, the Raman spectrum only shows bulk CuO. Any carbon species detected over the solid indicate that the copper species show an increased resistance to deactivation because they favor higher

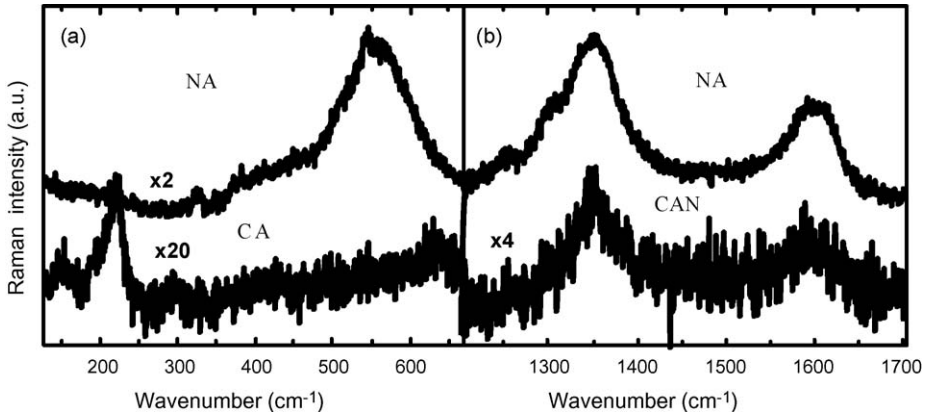

Fig. 8. Raman spectra of the spent catalysts used in dehydrogenation of ethylbenzene with CO_2 at 550 °C for 6 h of reaction at CO_2/EB = 30; (a) lower wavenumbers and (b) higher wavenumbers.

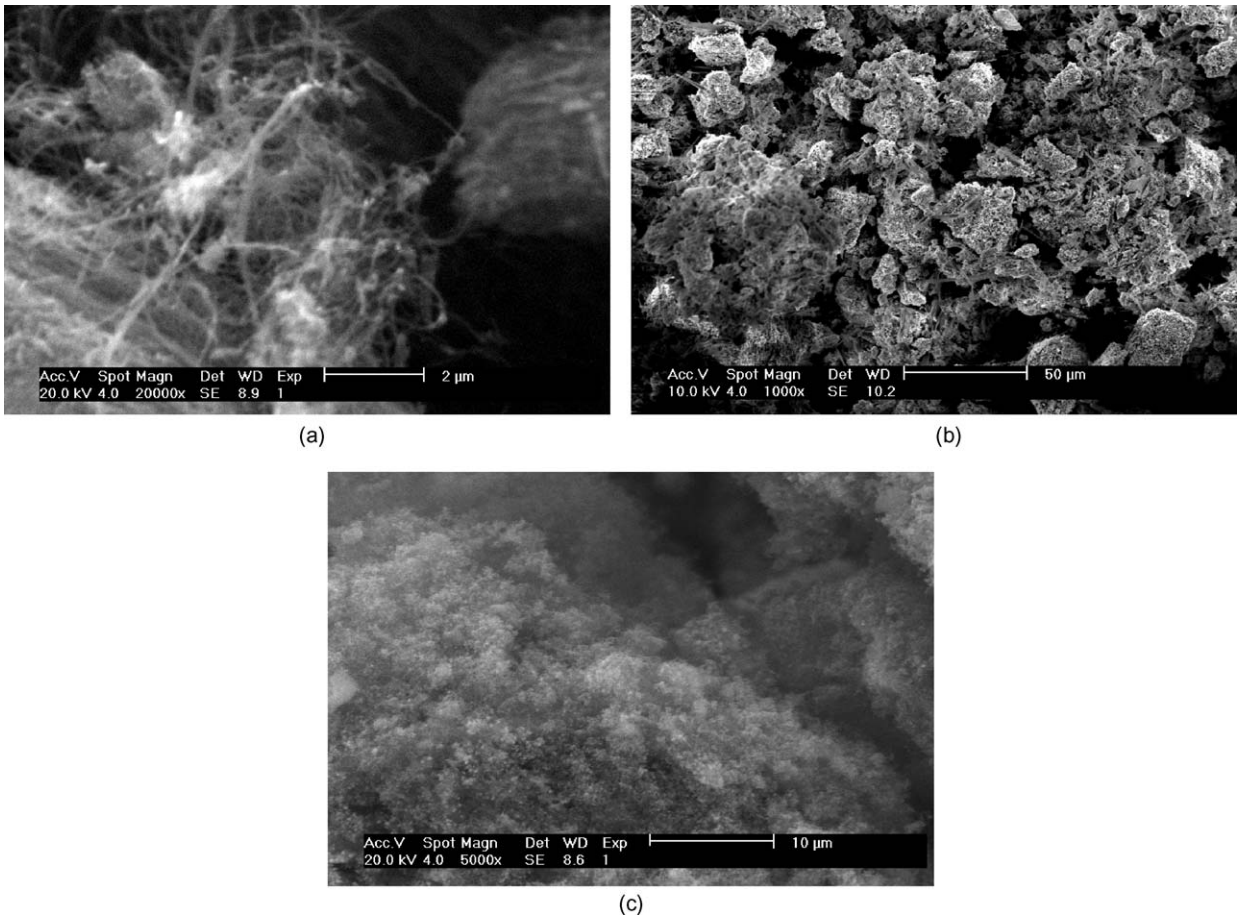

Fig. 9. SEM images of spent catalysts, used at 550 °C and CO_2/EB = 30. Samples: (a) NA, (b) CA and (c) CAN.

hydrogen mobility; as a consequence, this inhibits the formation of encapsulating carbon deposits, in accordance with the literature results [43]. However, the physical degradation of the catalyst (as seen by XRD) enhances carbon deposits in isolated phases on the surface (further observed by XPS). In fact, reactions (16) and (17) can occur, decreasing the carbon species over the solid:

$$C_6H_5CH = CH_2 \rightarrow \text{Precursors of coke} \quad (16)$$

$$\text{Precursors of coke} + H_2O \rightarrow CO + H_2 \quad (17)$$

Reaction (16) is an oligomerization that can lead to dehydrogenated coke. In contrast, reaction (17) is responsible for eliminating coke by a water gas shift reaction, avoiding coke deposition on the solid. Therefore, deactivation of CA in dehydrogenation of ethylbenzene is principally caused by the reduction of the copper species, in agreement with the previous XRD and TPR experimental observations.

In the case of CAN, the bands at 1253, 1352, and 1599 cm^{-1} (Fig. 8b) are typical of graphite and polyaromatic amorphous carbon [41,44]. No evidence of the reduced phases is observed due to the large amount of carbon on the solid surface. Copper favors carbon diffusion, since it has higher affinity for the graphene-based structure, and hence, it tends to inhibit the encapsulation of nickel sites by polyaromatic carbons in a Cu-Al-Ni alloy. Thus, this can explain the highest performance of CAN in comparison with CA.

NA presents a Raman spectrum characteristic of polycrystalline $NiAl_2O_4$, with a weak band at υ = 322, 378, 405, 446, 504, 540 and 571 cm^{-1} (Fig. 8a). Also, a broad band of medium intensity (between 504 and 540 cm^{-1}) represents the band of nickel aluminate spinels [44]. The main bands are situated at 1350 cm^{-1} (with a shoulder at 1252 and 1300 cm^{-1}) and 1600 cm^{-1}, as seen in Fig. 8b. The D-band at 1350 cm^{-1}, the disorder induced mode which corresponds to disordered graphite and carbons, comes from a symmetry lowering effect of the various carbon types on the surface during the catalytic test. The two relatively weak vibrational bands at 1300 cm^{-1} and 1350 cm^{-1} (Fig. 8b) are characteristic of the D-band disorder induced mode, most likely of sp^2 carbons activated by in-plane substitutional hetero-atoms, vacancies, grain boundaries or other defects [44]. The band at 1600 cm^{-1} indicates the existence of the graphite E_{2g} optic mode of highly crystalline materials. The high intensity of the band at 1350 cm^{-1} illustrates the large amount of carbonaceous disordered species as byproducts of the reaction. These results are in good agreement with XRD analysis, which shows a relatively large peak of graphite at $2\theta = 25.5^0$ in NA. The excess CO_2 probably oxidizes the carbon with graphene-based structures (filaments of carbon) continuously, while encapsulating some polyaromatic carbons on Ni active sites. Thus, NA has a low degree of reduction and carbon deposition, confirming the high performance of this solid. This will be also shown below by surface and morphological features of the spent catalysts.

3.3.2. Surface features and morphologies of spent catalysts

Morphological aspects of spent catalysts are shown by SEM images (Fig. 9).

As shown in Fig. 9a, spent $NiAl_2O_4$ catalyst is composed of tangles with a particle diameter of 8.8 nm, according to Raman measurements. Besides graphite features (filaments of carbon), large aggregates of particles can also be seen. In the case of CA (Fig. 9b), no carbon deposits are identified; only the solid structure

Table 5
Physico-chemical properties of the spent catalysts, used at 550 °C, N_2: 11.7 mmol h^{-1}; CO_2: 58 mmol h^{-1}; EB: 1.98 mmol h^{-1} (CO_2/EB ratio = 30).

Sample	BET surface area ($m^2\ g^{-1}$)	Pore volume ($cm^3\ g^{-1}$)	Coke amount [a] wt%	Particle size[b] (nm)	Intrinsic Activity (mol $m^2\ h^{-1}$) × 10^4
CA	13	0.10	1	12	2.5
NA	20	0.18	15	8.8	7.0
CAN	4	0.02	42	36.1	4.0

[a] From elemental analysis.
[b] From Raman measurements.

is noted. By contrast, the CAN image (Fig. 9c) documents the formation of carbon filaments that prejudice the selectivity of the solid in the reaction. Also, over Cu-Al-Ni, the structure, which is characteristic of this alloy, is not shown because of the excess of carbon filaments. SEM images confirm the different species of carbon deposited on NA and CAN spent catalysts. Any carbon deposition is detected over CA, in agreement with XRD and Raman results.

Additionally, Table 5 summarizes the textural properties of the spent catalysts. Pure CA possesses a low surface area (13 $m^2\ g^{-1}$), a relatively large pore volume (0.1 $cm^3\ g^{-1}$), and a moderate particle size (12 nm).

The drop in the surface area, compared to the values of fresh catalysts in Table 2, could be the result of a certain amount of CA pores blocked by large reduced particles of copper or by a carbon deposition of 1%. The agglomeration of copper species is probably the main cause of deactivation, whereas the slight carbon fouling is identified as the main consequence of the metal growth. Together these factors contribute to decrease the catalytic performance of the CA sample.

The textural parameter of CAN drastically deteriorates (BET surface area of 3 $m^2\ g^{-1}$ and particle size of 36.1 nm), which may be mainly attributed to the deposition of carbon (42%) on the catalyst, in accordance with elemental analysis, Raman and XRD experiments.

Studies on carbon nanotubes production via chemical vapor deposition on Ni/alumina catalysts show that at high Ni content, the internal forces between NiO and Al become weak. Hence, the reduction of Ni ions becomes easier, and carbonaceous deposits on the metal particles greatly increase [45]; as a consequence, Ni ions are more prone to congregate and Ni crystals grow larger, thus, the diameter of the particle may increase. However, it is not possible to confirm this result due to the high content of carbon on the solid. Nevertheless, no significant textural change is observed with spent NA catalyst, and this result reinforces the Raman and XRD results.

Interestingly, a relatively low amount of coke deposition is observed, confirming the hypothesis given for NA catalytic performance: non-deactivating carbon (filamentous carbon) that is not in close contact with the nickel particle limits the deactivation process on the catalyst surface.

The values of intrinsic activity at steady state condition were calculated from the area of spent catalysts. It is evident that the NA active surface (7.0×10^{-4} mol $h^{-1}\ m^2$) is more exposed to the reaction than CAN (4.0×10^{-4} mol $h^{-1}\ m^2$), and CA has a poor performance (2.5×10^{-4} mol $h^{-1}\ m^2$).

3.3.3. XPS of spent catalysts

The XPS analyses of spent catalysts are shown in Table 6.

The N and C samples are almost completely formed of Ni^0 and Cu^0, as strongly suggested by the binding energies for Ni $2p_{3/2}$ and Cu $2p_{3/2}$ at 852.5 and 932.5 eV, respectively. This confirms the previous XRD data. Indeed, the binding energy of Al 2p is 73.8 eV.

After the reaction, CA sample photoelectron lines due to Cu^0 (BE = 932.5 eV), CuO (BE = 933.6 eV), and to a lesser extent to $CuAl_2O_4$ (BE = 935.1 eV) were observed. Although the BE values of Cu $2p_{3/2}$ are spread over a fair interval in the literature, they can be assigned to the referred species [30]. These results evidence that the Cu^{1+} species observed on the surface of fresh CA sample (Table 3) are totally reduced to Cu^0. However, the low amount of Cu^{2+} as $CuAl_2O_4$ finely dispersed on the surface, together with bulk CuO, was not reduced after the catalytic test. Additionally, carbon traces were observed on the solid surface of the CA spent catalyst. This is in good agreement with Raman and elemental analyses that show any carbon over this sample. Therefore, it can be stated that the modest performance is due to sintering effects that provided the agglomeration of the particles and thus, an easy reduction. Because of their low stability in the reaction media, the remaining Cu^{2+} species are not able to restore the catalytic activity.

For NA, XPS results primarily indicate the presence of Ni^{2+} species (83%) on the surface that contribute to the enhancement of the catalytic activity for the ethylbenzene dehydrogenation. This confirms the hypothesis that $NiAl_2O_4$ (BE = 856.2 eV) is an active and stable phase that resists deactivation. BE of 855.4 eV assignable to NiO and also Ni^0 (BE = 852.3 eV) were found; however, the action of the latter specie did not contribute to improve the catalytic performance. Moreover, a BE corresponding to graphite-like carbon (BE = 285.7–288.9 eV, 66%) and 24% of filamentous amorphous carbon (BE = 282.1–284.3 eV) appear on the solid surface of the solid, in agreement with Raman and XRD results. As a consequence, these carbon species drop the surface area of the solid.

It is not surprising that difficult to eliminate coke, *i.e.* filamentous and amorphous carbons are deposited on Ni particles [41,46]. However, it is important to point out that the accumulation of these species on the surface is alleviated by CO_2 and the temperature of the reaction. Hence, carbonaceous deposits are

Table 6
Binding energy (BE), percentage of the species (in parenthesis) and percentage of metals (surface to bulk ratio) found on spent catalysts used at 550 °C, CO_2/EB = 30 and P = 1 atm.

Sample	Percentage			Percentage of metals (surface to bulk ratio)
	Ni $2p_{3/2}$	Cu $2p_{3/2}$	C1s	
N	855.3(20)[a] 852.5(80)[b]	–	–	0.3
C	–	933.7(10)[c] 932.5(90)[d]	–	0.1
CA	–	935.1 (11) 932.5 (66) 933.6 (23)	–	34.4
NA	855.4 (4) 856.2 (83) 852.3 (15)	–	282.1(7) 284.6(17) 286.7(12) 288.9(64)	6.1
CAN	852.3 (13) 856.2 (47) 855.3 (40)	935.0(66) 932.5(2) 933.9(32)	282.7(18) 284.3(51) 285.7(27) 288.4(4)	40.5[e]; 29.2[f]

[a] Ni^{2+}.
[b] Ni^0.
[c] Cu^{2+}.
[d] Cu^0.
[e] Copper species.
[f] Nickel species.

removed by the CO_2 present in the reaction mixture, leading to a stable performance of the NA catalyst, in comparison with the other solids.

XPS of spent CAN sample evidences the presence of a variety of oxidation states of the metals, such as Ni^{2+}, Cu^{2+}, Ni^0, and Cu^0, at 856.2 eV, 932.5 eV, 935.0 eV, and 852.5 eV, respectively. Among them, 47% of Ni^{2+} as $NiAl_2O_4$ and 40% as NiO were found, while 66% of Cu^{2+} as $CuAl_2O_4$ and approximately 32% of Cu^{2+} as CuO were also observed. It can thus be speculated that active nickel sites responsible for the activity are present in this solid. Nevertheless, the largest size of these particles on surface is a result of sintering that deteriorates the catalytic performance.

Indeed, a huge amount of deactivating carbon (BE = 282.7–288.4 eV) is formed on the surface of CAN, similarly to the NA sample. However, 69% of this coke is in the form of amorphous carbon that is difficult to remove by CO_2. In other words, over the CA sample, the decrease of the catalytic performance is associated with the reduction of the active component and the carbonaceous deposition on the solid surface. Additionally, the surface to bulk ratio values show that the surface availability of copper species is high for CA and CAN samples; the latter catalyst also has nickel species on the surface.

The XPS of spent catalysts show that deactivation of the studied catalysts is mainly due to the loss of active species and to the formation of coke on the solid surface that is not suppressed by an excess of CO_2. The $NiAl_2O_4$ active phase, on which CO_2 oxidizes Ni^{2+} species and eliminates the coke, is an exception. This is in agreement with Raman, XRD, SEM–EDX and elemental analysis experiments and can justify the better performance of NA catalyst.

3.4. Deactivation and recycling studies

3.4.1. Deactivation of the catalysts

The studies above demonstrate that deactivation by coking is the main factor responsible for the lack of activity of catalysts or their poor performance in ethylbenzene dehydrogenation. In order to evaluate whether the carbonaceous deposits alter the catalyst structure and properties, deactivation studies were carried out.

The dehydrogenation of ethylbenzene is studied at 550 °C at various CO_2/EB molar ratios and ambient pressure, and the results are shown in Fig. 10.

The reaction rates (molar flow rate/catalyst weight) are measured under stationary conditions. It is well established that introducing CO_2 instead of N_2, H_2, H_2O (vapor) and air during the

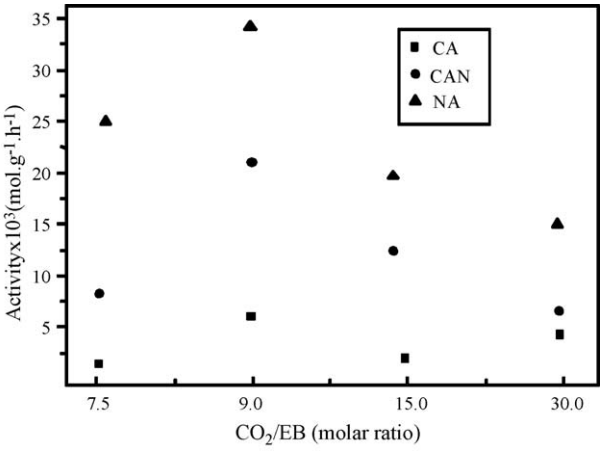

Fig. 10. Effect of CO_2/EB ratio on catalyst activity after 24 h of reaction. CO_2/EB ratio of 30 (N_2: 11.7 mmol h^{-1}; CO_2: 58 mmol h^{-1}; EB: 1.98 mmol h^{-1}), 15 (N_2: 11.7 mmol h^{-1}; CO_2: 29.7 mmol h^{-1}; EB: 1.98 mmol h^{-1}), 9 (N_2: 11.7 mmol h^{-1}; CO_2: 18.1 mmol h^{-1}; EB: 1.98 mmol h^{-1}) and 7.5 (N_2: 11.7 mmol h^{-1}; CO_2: 14.8 mmol h^{-1}; EB: 1.98 mmol h^{-1}).

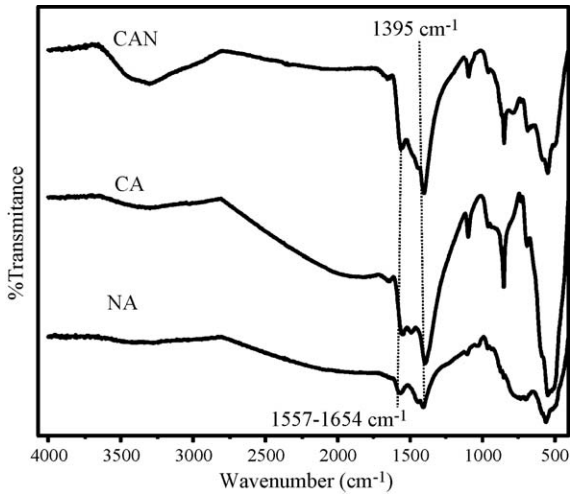

Fig. 11. FTIR of spent catalysts used at 550 °C and a CO_2/EB molar ratio of 9.

dehydrogenation of ethylbenzene [16] decreases coking by the decoking reaction:

$$\text{Coke} + CO_2 \rightarrow 2CO \quad (18)$$

Consequently, the activity of the catalyst will be stable because coking and decoking reactions reach an equilibrium [16,43–47].

As expected, NA, due to its stability, allows a higher extent of ethylbenzene conversion at the same level of activity, compared to CA and CAN. Activity reaches a maximum at a CO_2/EB ratio of 9, which is a typical behavior of consecutive reactions for all catalysts studied. The coking is a secondary reaction (reverse reaction (18)) that increases rapidly with the CO_2 content and decreases the activity at CO_2/EB = 30; other catalysts follow a similar behavior [17,19]. Therefore, although CO_2 can act as an oxidant, the large amount of the gas can cause the deactivation of the catalysts, as reported previously for iron oxide based catalysts [15].

FTIR spectra of the spent catalysts (Fig. 11) confirm the results observed at CO_2/EB = 9. The spectra exhibit a wide band related to O-H stretches of the steam produced during the reaction, which is observed in the range of 3200–3600 cm^{-1}. The C=C bands at 1557–1654 cm^{-1} are related to the vibration form of polyaromatics. Also, a = CH_2 band at 1395 cm^{-1}, corresponding to the C-H in-plane mode of the vinyl group from styrene, is identified for all catalysts studied [47].

Specifically, the band below 1395 cm^{-1} is more intense over spent CAN catalyst than over the other catalysts. This is indicative of an increase of styrene-adsorbed species on the solid in this condition.

To evaluate the causes of deactivation after 24 h of reaction, the coke deposition is analyzed by TGA experiments under air. Fig. 12 shows the TGA and also the DSC curve of spent NA at a CO_2/EB ratio of 30.

The TGA curve shows three distinct weight losses: the first, from 100 to 300 °C, corresponds to the loss of water and volatile materials adsorbed on the solid; the second, in the range of 600–900 °C, is related to the burning of easy-to-eliminate carbon species; the third, up to 1000 °C, is attributed to hard carbon deposits, *e.g.*, polyaromatic carbon species removal. In the DSC thermogram, these processes are characterized by two exothermic peaks and one endothermic peak, with approximate onset temperatures of 400 °C, 490 °C and 900 °C, respectively. Actually, the IR spectra of the released gas show a strong band at 2340 cm^{-1}, corresponding to CO_2, which is attributed to the burning of the carbon species. Furthermore, the gain in weight from 400 to 500 °C

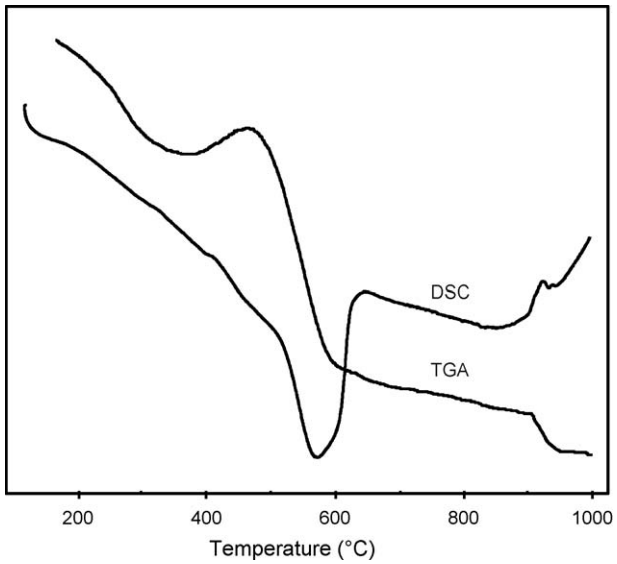

Fig. 12. TGA and DSC curves of spent NA tested at a CO_2/EB ratio of 30 and T = 550 °C.

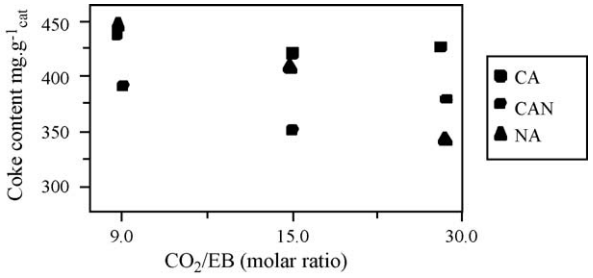

Fig. 13. Coke deposition as a function of the CO_2/EB ratio for 24 h of reaction.

is associated with the oxidation of nickel species. This was further confirmed by the green color of the particle, after the TGA experiment.

The results of the coke deposited over the solids as a function of the CO_2/EB ratio are shown in Fig. 13.

NA exhibits the highest coke production at CO_2/EB = 9 (445 mg g^{-1}_{cat}), followed by CAN (410 mg g^{-1}_{cat}), while CA has the lowest production (approximately 398 mg g^{-1}_{cat}). Increasing the CO_2/EB ratio does not provide a clear correlation to elucidate the role played by CO_2. However, higher CO_2 content does not alleviate coke formation after 24 h of reaction. It is likely that reaction (18) is occurring over this solid. However, the question remains of why less coke is produced over NA at higher CO_2/EB ratios. This apparent contradiction is explained by the fact that on this sample, larger amounts of CO_2 (by consuming EB) converted to side products lead to less coke deposited on the solid. As selectivity to styrene is much higher with the NA sample at CO_2/EB = 30 and 550 °C (Table 4), a continuous reoxidation of the surface Ni^{2+} species in the aluminate matrix by excess CO_2 is suggested. Therefore, reaction (17) may be occurring over NA. In the cases of CA and CAN, heavy carbonaceous deposits contribute to deactivation, independently of the CO_2/EB ratio studied.

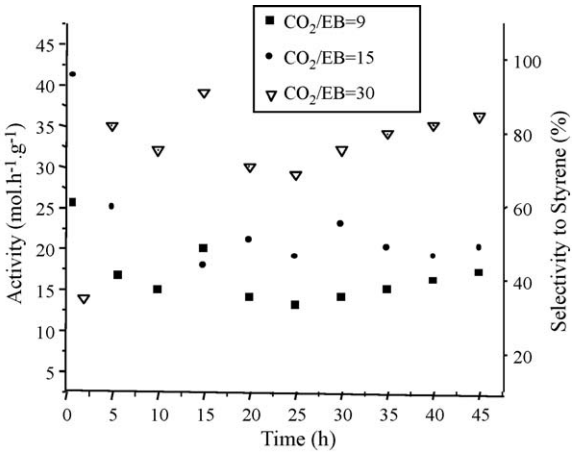

Fig. 14. Deactivation of NA recycled catalyst. Activity and selectivity vs. time on-stream, under 550 °C and 1 atm of pressure.

Deviating from previous results, the activity of dehydrogenation of ethylbenzene is found to be greatly improved by using CO_2 due to the simultaneous elimination of hydrogen generated by ethylbenzene dehydrogenation, which would otherwise reduce the active site of the catalyst. Therefore, CO_2 is not able to suppress coke production, but it maintains the high oxidation state of the catalyst.

3.4.2. Catalyst recycling

The catalysts deactivated at CO_2/EB = 30 (spent catalyst) were tentatively activated with CO_2 without ethylbenzene for 1 h in order to determine the recycling ability of the catalysts.

From thermal analysis obtained using CO_2, the weight loss steps (not shown) indicate the elimination of carbon deposits on the NA surface. From DTA curves, two types of carbons are formed on NA. The first one, at approximately 517 °C, indicates graphite-like carbon on a solid surface, as shown with a Ni-based catalyst for methane reforming [46–49].

The strongest peak at 597 °C is related to filamentous carbon with a graphite structure, while polyaromatic carbons are identified at 900 °C [49]. FTIR spectra also registered the total combustion of the hydrocarbons to produce carbon dioxide and water. After burning the solid at 1000 °C, the catalyst becomes green, similar to the initial solid. The percentage of carbon deposited is estimated from TGA curves in Table 7, which shows the coke content of regenerated catalyst at CO_2/EB of 30.

The catalytic performance of regenerated $NiAl_2O_4$ is deeply depressed (Fig. 14).

From Fig. 14, a considerable increase in the initial activity is seen at different CO_2/EB ratios, which is consistent with the lower amount of coke formed at CO_2/EB ratio = 30. As CO_2 is formed, coke production is diminished. However, activity gradually decreases with the progress of the reaction. Moreover, styrene selectivity decreases in the first 10 h of reaction at CO_2/EB = 15 and 30. The catalyst has similar tendencies in decreasing the activity. However, at a CO_2/EB molar ratio of 9, activity decays slowly with the time on-stream until 30 h of reaction. As the reaction proceeds, the selectivity to styrene reaches 45% at a CO_2/EB ratio of 9.

Table 7
Characterization of the regenerated catalysts (recycling test). The reaction is carried out at 550 °C, CO_2/EB = 30 and P = 1 atm, during 6 h.

Sample	Activity (mol g^{-1} h^{-1}) × 10^3	% Styrene selectivity	BET surface area (m^2 g^{-1})	% Residual coke amount	Particle size (nm)
CA	2.8	55.0	17	1.0	27
NA	0.8	69.5	10	0.6	23
CAN	11.8	74.8	3	8.4	29

When the CO_2/EB ratio increases, the rate of coupling reaction (9) increases; as a consequence, the production of water and CO greatly increases with reaction time. By contrast, styrene and hydrogen yields decrease. This lack of CO_2 to convert ethylbenzene explains the low selectivity to styrene, as the reaction occurs in a single step.

Furthermore, the coke contents on spent catalysts after 40 h of reaction were 383, 350 and 375 mg g^{-1} (From TGA analysis), respectively for CO_2/EB = 9, 15 and 30. This confirms that the carbon deposits on the surface of the catalysts continuously increase as the reaction proceeds, and it also demonstrates that the activity of the solids is sensitive to nickel particle growth and carbon deposition. However, deactivation due to coke may be reduced by introducing a large amount of CO_2. By using a CO_2/EB ratio of 30, selectivity to styrene is greater, and less carbon (in the form of graphite or polyaromatics) is formed.

Although the most suitable condition for dehydrogenation of ethylbenzene is a CO_2/EB molar ratio of 30, a temperature of 550 °C and 1 atm of pressure, the catalytic activity is accompanied by rapid deactivation of the catalyst due to coking. Doping of NA with sodium was carried out in order to reduce the surface acidity, which in turn was expected to reduce coking and increase the activity; however, this did not succeed.

Based on FTIR, XPS and Raman studies, coke originates on the solid surface during the reaction. The coke forms are aliphatic and polyaromatic carbons [4], the latter being, quantitatively, the main species of coke (from TGA analysis). Over CAN and NA, polyaromatic carbon deposits are severe, whereas over CA, the amount of this carbon species is fairly appreciable.

The regenerated catalysts were again submitted to CO_2 treatment *in situ*, and accelerated experiments were carried out for an additional 6 h of reaction. After this period, the catalyst returns the nickel or copper to a specific area of its fresh values. In order to understand this phenomenon, the results are shown in Table 7 under the heading of recycling tests.

As expected, NA and CAN, due to their relative ability of regeneration, exhibit a much higher activity than CA (0.8×10^{-3} mol g^{-1} h^{-1}). One piece of evidence for regeneration of the solids is the pale-green catalyst particle, which has a gray layer after the recycling studies, which is an indication of Ni^{2+} species (in NA) and Ni^{2+} and Cu^{2+}species for CAN. The catalyst performance observed in Table 7 is comparable to that of Table 4 for the same condition studied. However, the selectivity is smaller compared to the fresh catalyst. A low styrene yield can be the result of the lower availability of O^- sites, which abstract the α-hydrogen of ethylbenzene, due to particle growth after regeneration studies (respectively 23 and 29 nm) for NA and CAN.

However, in the case of CAN, a mixture of red and black particles may indicate Cu^0 species and coke, respectively. Also, CA regeneration does not occur because the oxidant atmosphere cannot suppress the deep reduction of the Cu^{2+} species. As Cu^0 is unable to convert ethylbenzene, the activities drastically decay. This is consistent with the decrease in the surface area of this catalyst after the recycling test by analyzing the textural features of the fresh catalysts (Table 3). Coke deactivation over a CA sample is unlikely, as proven by the residual content of carbon after the second recycling of this solid and observed by XPS and SEM–EDX of spent catalyst. Thus, direct transformation of EB to styrene and hydrogen is possible (reaction (8)) over CA.

Another reason for the non-preferential formation of styrene is that once this aromatic is formed, it is preferably transformed to graphitic filaments, or coke, on Ni^{2+} sites, in the cases of CAN and NA recycled samples. The CO and water yields increase slightly with the presence of nickel, because oxygen from CO_2 is used to maintain the nickel oxidation state. More CO is formed in the reaction media, and it reacts with H_2, producing CO_2 and water (reaction (19)).

$$CO + H_2 \rightarrow CO_2 + H_2O \quad (19)$$

Styrene is formed during the direct transformation of ethylbenzene (reaction (8)), and it does not desorb rapidly from Ni^{2+} sites. Subsequently, the molecules of styrene accumulate in a dimer form (stylbene) over the Ni^{2+} sites; thereafter, carbonaceous deposits increase steadily with time.

NA shows a decrease in carbon deposition because Ni^{2+} species are prone to producing graphite carbon, which is easy to eliminate, without affecting the conversion of ethylbenzene. On the other hand, polyaromatic carbons cannot be burned by CO_2 during the reaction, and the catalyst experiences a gradual deactivation in comparison with fresh NA catalyst. This results in a decay of styrene selectivity, as compared with the values of fresh NA selectivity (Table 4).

CAN has the same ability as NA, but reduction of copper particles is the primary cause of deactivation. As Cu^{2+} donates electrons to maintain Ni^{2+} species, the martensite phase (Cu-Al-Ni) is stabilized on the solid surface; in contrast, the action of such a phase cannot eliminate carbon deposition, even if CO_2 is present. Therefore, the cycle mechanism mentioned above for NA, is valid for CAN recycled catalyst. Coke formation over CAN is the main cause of deactivation, as seen by the 8.4% of carbon deposits over the recycled solid. Consequently, surface area and catalytic performance drastically change, in comparison with the parent fresh catalyst. Conversely, NA undergoes performance improvements due to the amount of coke formed, which is filamentous graphitic carbon instead of polyaromatics. Since the latter is difficult to eliminate, it hinders the catalytic activity and selectivity of the recycled catalyst for ethylbenzene dehydrogenation. In addition, styrene selectivity is lower than that of fresh samples; however, an inspection of the solid after regeneration showed that the Ni^{2+} active sites rest due to the contribution of CO_2 from the reaction. This assures $NiAl_2O_4$ as the active phase for catalyzing the ethylbenzene dehydrogenation with CO_2. Therefore, over $NiAl_2O_4$ phase, the direct dehydrogenation of ethylbenzene takes place, while the coupling reaction is responsible for reoxidizing the catalyst.

4. Conclusions

$NiAl_2O_4$ is a suitable phase for the dehydrogenation of ethylbenzene with CO_2 in comparison to Cu-Al-Ni and $CuAl_2O_4$. Pure NiO and CuO are practically inactive in the reaction due to the reduction of the metal species.

Nickel aluminate oxygen defects are oxidized by CO_2; however, the gas does not alleviate coke formation. Over $CuAl_2O_4$, Cu^{2+} reduction is the main reason for the deactivation of the catalyst, as proved by XPS. Moreover, in the case of mixed nickel and copper aluminates there is a synergistic donation of electrons between Cu^{2+} and Ni^{2+} that contributes to the formation of a stable ternary system (Cu-Al-Ni). However, this does not eliminate the reduction of copper in the aluminate alloy; consequently, a deeper reduction of the active $NiAl_2O_4$ phase added to carbonaceous deposits causes the deactivation of the catalyst during the dehydrogenation of ethylbenzene with CO_2.

Deactivation and recycling studies of the $NiAl_2O_4$ catalyst show that the nature of coke is closely related to the activity and styrene selectivity. Filamentous graphite carbon (observed by Raman, XPS and SEM–EDX analyses) is easily removed from the solids, while polyaromatic carbon can cover the active sites and thus decrease the catalytic activity.

The addition of CO_2 regains the oxidation state of reduced Ni species, but it cannot eliminate the heavy hydrocarbons during

reaction. The $NiAl_2O_4$ activity is directly related to the structural and textural properties of the solid. This catalyst showed a fixed stability with respect to the carbon deposition, without significantly affecting the selectivity.

Among the conditions studied, the CO_2/EB = 30 at relatively low temperature (550 °C) and 1 atm of pressure is a suitable condition to perform the direct transformation of ethylbenzene to styrene, whereas coupling reactions have a secondary role in the re-oxidation of the active phase over $NiAl_2O_4$. Activity of $NiAl_2O_4$ was comparable to that of Fe-K commercial catalyst for dehydrogenation, leading over the steam [16].

Acknowledgements

This work was sponsored by CNPQ. We acknowledge Prof. J.M. Sasaki for the XRD analysis. Also, we acknowledge Prof. A.G. Souza-Filho as well as Prof. A. Valentini for valuable discussions. We are also thankful to J.J. Hiluy Filho for A. L. P. assistence.

References

[1] E.H. Lee, Catal. Rev. Sci. Eng 8 (1983) 285–305.
[2] K.K. Kearby, US Patent 2,370,797 (1945).
[3] W.D. Mross, Catal. Rev. Sci. Eng. 25 (1983) 591–637.
[4] F. Cavani, T. Trifirò, Appl. Catal. A: Gen. 133 (1995) 219–239.
[5] A.C. Oliveira, A. Valentini, P.S. Nobre, M.C. Rangel, Catal. Today 2003 (2003) 49–57.
[6] H. Li, Y. Yue, C. Miao, Z. Xie, W. Hua, Z. Gao, Catal. Commun. 8 (2007) 1317–1322.
[7] G.R. Meima, P.G. Menon, Appl. Catal. A: Gen. 212 (2001) 239–245.
[8] B.S. Liu, G. Rui, R.Z. Chang, C.T. Au, Appl. Catal. A: Gen. 335 (2008) 88–94.
[9] M. Surgino, H. Shimada, T. Turuda, H. Miura, N. Ikenaga, T. Suzuki, Appl. Catal. A: Gen. 121 (1995) 125–137.
[10] N. Mimura, M. Saito, Catal. Today 55 (2000) 173–178.
[11] Y. Ohishi, T. Kawabata, T. Shishido, K. Tanaki, Q. Zhang, Y. Wang, K. Takehira, J. Mol. Catal. A. Chem. 230 (2005) 49–58.
[12] G. Carja, Y. Kameshima, K. Okada, Microp. Mesop. Mater. 115 (2008) 541–547.
[13] J.R. Bispo, A.C. Oliveira, S.G. Marchetti, M.C. Rangel, Stud. Surf. Sci. Catal. 142 (2002) 517–524.
[14] X. Ye, N. Ma, W. Hua, Y. Yue, C. Miao, Z. Xie, Z. Gao, J. Mol. Catal. A: Chem. 217 (2004) 103–108.
[15] A. Sun, Z. Qin, J. Wang, Appl. Catal. A: Gen. 234 (2002) 179–189.
[16] A. Miyakoshi, A. Veno, M. Ichikawa, Appl. Catal. A: Gen. 216 (2001) 137–146.
[17] N.J. Jebarathinan, M. Eswaramoorthy, V. Krishnasamy, Appl. Catal. 145 (1996) 57–74.
[18] D.-Y. Hong, V.P. Vislovskiy, Y.K. Huang, S.H. Jhung, J.-S. Chang, Catal. Today 131 (2008) 140–145.
[19] S. Chen, Z. Qin, A. Sun, J. Wang, J. Nat. Gas Chem. 15 (2006) 11–20.
[20] B. Xiang, H. Xu, W. Li, Chin. J. Catal. 28 (2008) 841–843.
[21] A.L. Pinheiro, R.M. Freire, E. Longhnotti, A.C. Oliveira, in: Proceedings in Simposio Iberoamericano de Catalisis, Málaga, Spain, 2008.
[22] L.G. Cançado, K. Takai, T. Enoki, A. Jorio, L.N. Coelho, R. Magalhães, Appl. Phys. Lett. 88 (2006) 163106–163109.
[23] G.A. El-Shobaky, N.R.E. Radwan, M. Samy El-Shall, A.M. Turky, H.M.A. Hassan, Colloids Surf. A: Physicochem. Eng. Aspects 311 (2007) 161–169.
[24] K. Tonooka, K. Shimokawa, O. Nishimura, Thin Solid Films 411 (2002) 129–133.
[25] Y.S. Han, J. Bao Li, X. Shan, N. Xiao, Z. Yang, B. Chi, Mater. Sci. Eng. A 369 (2004) 241–244.
[26] A. Aydogdu, Y. Aydogdu, O. Adiguzel, J. Mater. Process Technol. 153 (2004) 164–169.
[27] U. Sarı, T. Kırındı, Mater. Character 59 (2008) 920–929.
[28] A. Al-Ubaid, E.E. Wolf, Appl. Catal. 40 (1988) 73–85.
[29] J. Requies, M.A. Cabrero, V.L. Barrio, J.F. Cambra, M.B. Güemez, P.L. Arias, V. La Parola, M.A. Peña, J.L.G. Fierro, Catal. Today 116 (2006) 304–312.
[30] P.A. Kumar, M.P. Reddy, L.K. Ju, B. H.-Sook, H.H. Phil, J. Mol. Catal. A: Chem. 291 (2008) 66–74.
[31] T.-L. Lai, W.-F. Wang, Y.-Y. Shu, Y.-T. Liu, C.-B. Wang, J. Mol. Catal. A: Chem. 237 (2007) 304.
[32] K.V.R. Chary, K.K. Seel, D. Naresh, P. Ramakanth, Catal. Commun. 9 (2008) 77–81.
[33] N.J. Jebarathinan, M. Eswaramoorthy, V. Krishnasamy, Bull. Chem. Soc. Jpn. 67 (1994) 3334–3338.
[34] M.F. Luo, Y.J.Z. Hong, X.X. Yuan, X.M. Zhong, Appl. Catal. A.: Gen. 162 (1997) 121–131.
[35] M.-F. Luo, P. Fang, M. He, Y.-L. Xie, J. Mol. Catal. A: Chem. 239 (2005) 243–248.
[36] J. Dussault, J.C. Dupin, N. Latone, T. Ubieto, L. Noé, M. Monthioux, E. Romero, C. Royo, A. Monzón, C. Guimon, J. Phys. Chem. Sold 67 (2006) 1162–11670.
[37] S. Kurien, J. Mathew, S. Sebastien, S.N. Potty, K.C. George, Mater. Chem. Phys. 98 (2006) 470–476.
[38] C. Kuhrs, Y. Arita, W. Weiss, W. Ranke, R. Schlogl, Top. Catal. 14 (2001) 111–123.
[39] D. Zhang, L. Shi, F. Fang, X. Li, K. Dai, Mater. Lett. 59 (2005) 4044–4047.
[40] C. Li, M.J. Li, J. Raman Spectosc. 33 (2002) 301–308.
[41] A.N. Pinheiro, A. Valentini, J.M. Sasaki, A.C. Oliveira, Appl. Catal. A: Gen. 355 (2009) 156–168.
[42] J.F. Xu, W. Ji, Z.X. Shen, W.S. Li, S.H. Tang, X.R. Ye, D.Z. Jia, X.Q. Xin, J. Raman Spectrosc. 30 (1999) 413–415.
[43] Y. Li, L. Chang, Y. Qin, J. Catal. 178 (1996) 76–83.
[44] M.A. Laguna-Becero, M.L. Sanjuán, R.I. Merino, J. Phys. Condens. Matter. 19 (2007) 186217–186227.
[45] H. Li, C. Shi, X. Du, C. He, J. Li, N. Zhao, Mater. Lett. 62 (2008) 1472–1475.
[46] B. Pawalec, S. Damyamova, K. Arishtiova, J.L.G. Fierro, L. Petrov, Appl. Catal. A: Gen. 323 (2007) 188–201.
[47] M. Baghalha, O. Ebrahimpour, Appl. Catal. A: Gen. 326 (2007) 143–151.
[48] F. Peng, X.-B. Fu, H. Yu, H.-J. Wang, New Carbon Mater. 22 (2007) 213–217.
[49] J.H. Kim, D.J. Suh, T.J. Park, K.L. Kim, Appl. Catal. A: Gen. 197 (2000) 191–200.